FOI-R--1533--SE
December 2004
1650-1942

Scientific report

Pontus von Schoenberg

Development of a Large-Eddy Simulation code for the atmospheric boundary layer

NBC Defence Division
SE-901 82 UMEÅ
Sweden

Swedish Defence Research Agency
NBC Defence Division
SE-901 82 UMEÅ
Sweden

FOI-R--1533--SE
December 2004
1650-1942

Scientific report

Pontus von Schoenberg

Development of a Large-Eddy Simulation code for the atmospheric boundary layer

Issuing organization	Report number, ISRN	Report type
Swedish Defence Research Agency NBC Defence Division SE-901 82 UMEÅ Sweden	FOI-R--1533--SE	Scientific report
	Research area code: 3 NBC Defence and other hazardous substances	
	Month year: December 2004	Project no.: A 4521
	Subcategory: 32 Biological and Chemical Defence Research	
	Subcategory 2:	

Author/s (editor/s)	Project manager
Pontus von Schoenberg	Lennart Thaning
	Approved by: Åsa Fällman
	Sponsoring agency:
	Scientifically and technically responsible:

Report title

Development of a Large-Eddy Simulation code for the atmospheric boundary layer

Abstract

A Large-Eddy Simulation (LES) code, previously not used for simulating the Planetary Boundary Layer (PBL), has been developed to take atmospheric conditions into account. The LES has been tested for a neutral, stable and unstable PBL. The neutral simulation has been compared with previous studies and shows satisfactory results. The unstable simulation indicates that the implemented code works correctly, but further evaluation has to be done. The same is true for the stable simulation.

Keywords

Large-Eddy Simulation, LES, Planetary Boundary Layer,PBL, Meteorology, Turbulence

Further bibliographic information	Language
Extended version of a Degree project, master of Science, Meteorology, 20p. Department of Meteorology, University of Stockholm(MISU). Supervisors: Michael Tjernström (MISU), Lennart Thaning(FOI).	English
ISSN: 1650-1942	Pages: 33
Distribution: By sendlist	Price: Acc. to pricelist Security classification: Unclassified

Utgivare	Rapportnummer, ISRN	Klassificering
Totalförsvarets forskningsinstitut Avdelningen för NBC-skydd SE-901 82 UMEÅ Sweden	FOI-R--1533--SE	Vetenskaplig rapport
	Forskningsområde: 3 Skydd mot NBC och andra farliga ämnen	
	Månad, år: December 2004	Projektnummer: A 4521
	Delområde: 32 B- och C-forskning	
	Delområde 2	

Författare/redaktör	Projektledare
Pontus von Schoenberg	Lennart Thaning
	Godkänd av: Åsa Fällman
	Uppdragsgivare/kundbeteckning
	Tekniskt och/eller vetenskapligt ansvarig

Rapportens titel

Utveckling av en "Large-Eddy Simulation" kod för atmosfärens gränsskikt

Sammanfattning

En "Large-Eddy Simulation" (LES) kod som tidigare inte används för atmosfärens gränsskikt har utvecklats för att inkludera atmosfäriska egenskaper. LES-koden har testats och verifierats för ett neutralt, ett instabilt och ett stabilt gränsskikt. Den neutrala simuleringen har jämförts med tidigare studier och visar ett positivt ressultat. Den instabila och stabila simuleringen indikerar att koden arbetar korrekt, men fortsatta undersökningar måste utföras. Det samma gäller för den stabila simuleringen.

Nyckelord

Large-Eddy Simulation, LES, Atmosfärens Gränsskikt, Meteorologi, Turbulens

Övriga bibliografiska uppgifter	Språk
Utökad version av ett 20p fil. mag. examensarbete i Meteorologi.Meteorologiska Institutionen, Stockholms Universitet (MISU). Handledare:Michael Tjernström (MISU), Lennart Thaning (FOI).	Engelska
ISSN: 1650-1942	Antal sidor: 33
Distribution: Enligt missiv	Pris: Enligt prislista Sekretess: Öppen

Contents

1. Introduction

Large Eddy Simulation (LES) is a useful tool for the study of turbulent flows. With increasing computer power and parallel processor supercomputers LES is considered to become a powerful tool in the future. In LES the flow is separated into large and small scale motions where the large scales contain the main part of the turbulence and energy containing structures. The large scale structures are resolved in LES and calculated explicitly while the small scale motions are modelled or parameterized. The large scale motions are believed to be more dependent on the flow environment than the small scale motions which are considered to have a more universal character. The LES results are believed to be relatively insensitive to the small scale, or Sub Grid Scale (SGS), parameterization scheme.

The topic for this study is to investigate a LES code previously not applied for atmospheric flows. The LES code will be tested and compared with results from other LES studies in the atmosphere. Different types of planetary boundary layers, neutral, unstable and stable, are simulated. The experiments with a neutral boundary layer is compared with results from Andrén et al. [1994]. The simulation of the stable boundary layer is compared with studies by Andrén [1995].

The LES code that has been used is built with a C++ class library called FOAM, "Field Operation And Manipulation" (Weller et al. 1988a, 1988b). FOAM is created with the purpose to make it easy to solve a set of complex partial differential equations and in particular, development of reliable and efficient codes for computational continuum dynamics. When writing codes with FOAM, the equations are made to resemble the original equations as much as possible and the notations for tensors and differential equations is on the top level close to conventional mathematical notation. Object orientated programming techniques make it possible to enable data types to work very similar to continuum mechanics.

2. Numerical Models for Fluid dynamics

There are many ways to simulate fluid motions numerically. Most simulations or models use the Navier-Stokes Equations (NSE), either direct or after an appropriate averaging. Ensemble Average Models (EAM) use an averaged set up of NSE. Assuming that the interesting features of the flow lies in the mean field, only the mean field is calculated and all deviations are parameterized. EAM has been used in many engineering and environmental studies. All turbulence, also that which in principle could be resolved, is parameterized in the EAM code. Ensemble average models can only be used when the mean values are the interesting part of the study, but they are computationally efficient tools compared to for example Direct Numerical Simulation (DNS). DNS is a direct approach to solve the complete set of Navier Stokes equations. Here a fine grid resolution is used in order to resolve all turbulent motions (i.e. down to $\sim$ 1 mm.). This technique is computationally very expensive and it is only now, in the age of the super computers that DNS has become possible. Still it has only been used for flows with low Reynolds numbers. To simulate the turbulence in the atmosphere a different tool is needed.

For atmospheric simulations the wether prediction models resolves large scales and parameterize small scales. Large scales in this context are considered to be the synoptic scale motions such as the low pressure systems coming in from the Atlantic, passing northern Europe. All turbulence are in these models parameterized. When simulating phenomena on smaller scales the distinction between large and small scales has to be changed.

When studying features in the Planetary Boundary Layer (PBL) the turbulence is of greatest importance. In Large Eddy Simulation (LES) the large eddies are resolved and simulated while the small eddies are parameterized or modelled. The large eddies are considered to be those that contain most of the turbulent kinetic energy in the flow and take care of the main part of the transport of parameters such as heat and momentum. Eddies smaller than the resolution must be parameterized in a SGS model. This way of calculating fluctuations and turbulence is computationally reasonable. Depending on what is going to be investigated, different computational methods have their different advantages. For planetary boundary layer simulations LES is a good tool.

One of the earliest successful attempts with LES for the atmosphere was made by Deardorff in the 1970:s with simulations of the convective boundary layer [Deardorff, 1973]. The convective boundary layer has been more successfully simulated compared to the neutral and stable boundary layers. The convective boundary layer is dominated by large fluctuations that are well resolved in the LES domain. Most of the energy is located within the large scales which makes the LES insensitive to the sub grid scale fluctuations and therefore less dependent to the difficulties with sub grid scale modelling.

In the neutral boundary layer there are no temperature differences. This makes it easier to simulate because the temperature equation is not needed. In the simulation made for the neutral PBL in this study, the temperature equation is still retained in the code but since there are no temperature differences in the field, it takes no part in the calculations. LES for the neutral boundary layer are well documented and understood, for industrial purposes, but not as thoroughly investigated for the atmosphere. The results for the neutral simulation is compared to the results of Andrén et al. [1994].

A test for a slightly stable boundary layer is also performed. This is the most challenging boundary layer to simulate. In a stable atmosphere the turbulence is very week and the scale is small. This means that the eddies in the domain are very small and large parts of them are not resolved, especially close to the ground. Even energy

containing eddies are not resolved which is the basic idea with the LES approach. The LES is consequently more dependent of the parameterization scheme which already is one of the crucial and difficult parts of the LES code. In this field there is much to be done before LES behaves satisfactory according to observations. The stable simulation is compared with Andrén [1995].

3. Theory

The LES code investigated in this theses is built with the C++ library FOAM and will henceforth be referred to as FOAM. Here the basic equations and assumptions used in FOAM will be described together with the grid setup and differentiation scheme.

3.1 Basic Equations

Motions in a flow are believed to be adequately described by Navier Stokes equations. They may be written in tensor form as [Stull, 1988, section 3.2.3]:

$$\frac{\partial u_i}{\partial t} + u_j \frac{\partial u_i}{\partial x_j} = -\delta_{i3} g - 2\varepsilon_{ijk}\Omega_j u_k - \frac{1}{\rho}\frac{\partial p}{\partial x_i} + \frac{1}{\rho}\frac{\partial \tau_{ij_{visc}}}{\partial x_j} \tag{3.1}$$

This is an equation for the velocity vector $u_i = (u, v, w)$, where δ and ε are the Kronecker delta and the alternating unit tensor (see Appendix 6.1 for details). Ω is the earth rotation, $\Omega = (0, \omega\cos\varphi, \omega sin\varphi)$, where φ is the latitude and ω is the angular rotation velocity of earth. Thus is both horizontal and vertical coriolis force included in the code. Further variables are earth gravity g, pressure p, air density ρ and the viscous stress tensor, $\tau_{ij_{visc}}$ further discussed in Appendix 6.2. The variables are functions of time, t and space, $x_j = (x, y, z)$. The orientation is for x eastwards, along a latitude, for y northwards, along a longitude, while z is vertical.

To close the problem we include the *continuity equation*, Equation 3.2. Assuming that the atmosphere is incompressible, $\frac{d\rho}{dt} \equiv 0$, the continuity equation may be simplified as:

$$\frac{\partial \rho}{\partial t} + \frac{\partial \rho u_j}{\partial x_i} = \frac{\partial \rho}{\partial t} + u_i\frac{\partial \rho}{\partial x_i} + \rho\frac{\partial u_i}{\partial x_i} = \frac{d\rho}{dt} + \rho\frac{\partial u_i}{\partial x_i} = 0 \tag{3.2}$$

$$\Rightarrow \frac{\partial u_i}{\partial x_i} = 0 \tag{3.3}$$

The thermodynamical equation is also needed for the PBL simulations.

$$\frac{\partial \theta}{\partial t} = -u_j\frac{\partial \theta}{\partial x_j} - \frac{\partial \tau_{\theta j_{visc}}}{\partial x_j} + Source \tag{3.4}$$

where θ is the potential temperature and $\tau_{\theta j}$ is the flux of potential temperature. An equation of state for dry air is further assumed:

$$P = \rho R T \tag{3.5}$$

where $R = 287.05\frac{J}{kg\cdot K}$. Equations 3.1 - 3.5 mathematically closes the problem. They describe the motions in a fluid. They can, however, not be solved analytically, which is why a numerical approach is used.

3.2 Further Assumptions

The thermodynamic variables is separated into a "reference state" and deviations from this 'reference state" i.e. $T = T_0 + T_1$, $\rho = \rho_0 + \rho_1$ and $p = p_0 + p_1$. It is assumed that the atmosphere at rest is in hydrostatical balance and that deviations from the "reference state" are much smaller than the "reference state" itself, $T_1 << T_0$, $\rho_1 << \rho_0$ and $p_1 << p_0$, the *Boussinesq assumptions*, see e.g. Arya [1988, section 7.7.2]. Hydrostatical balance may be written in terms of the "reference state":

$$-g\rho_0 = \frac{\partial p_0}{\partial z} \tag{3.6}$$

Furthermore it is assumed that $\frac{\rho_1}{\rho_0} = -\frac{T_1}{T_0} = -\frac{\theta_1}{\theta_0}$ which is a good approximation when the wind speed is much less than the speed of sound. Using the these assumptions the Navier stokes equations may now be rewritten as:

$$\frac{\partial u_i}{\partial t} + u_j \frac{\partial u_i}{\partial x_j} = -2\epsilon_{ijk}\Omega_j u_k - \frac{1}{\rho_0}\frac{\partial p_1}{\partial x_i} + \delta_{i3} g \frac{\theta_1}{\theta_0} + \frac{1}{\rho}\frac{\partial \tau_{ij_{visc}}}{\partial x_j} \tag{3.7}$$

often referred to as the Boussinesq approximated Navier Stokes equations. The variables are separated in two parts, one that is to be resolved in the model and one that deviates from the resolved part; $u = \bar{u} + u'$, $p = \bar{p} + p'$ and $\theta = \bar{\theta} + \theta'$. The resolved part, or in our case the grid box average, is denoted with $\bar{}$ and the deviation from these, the sub grid scale part, is denoted with $'$.

Then averaging rules are applied to the equations [1] [compare with Arya, 1988, section 9.1.3]. Using the averaging rules and the incompressible version of the continuity equation, the following expression for Navier Stokes equations may be derived [see Deardorff, 1974]:

$$\frac{\partial \bar{u}_i}{\partial t} + \frac{\partial \bar{u}_i \bar{u}_j}{\partial x_j} = -2\epsilon_{ijk}\Omega \bar{u_k} - \frac{1}{\rho_0}\frac{\partial \bar{p}_1}{\partial x_i} + \delta_{i3} g \left(\frac{\bar{\theta} - \tilde{\theta}}{\theta_0}\right) - \frac{\partial \overline{u_i' u_j'}}{\partial x_j} + \frac{1}{\rho_0}\frac{\partial \tau_{ij_{visc}}}{\partial x_j} \tag{3.8}$$

where $\tilde{\theta}$ is a mean value of the potential temperature which in FOAM is calculated as a time average of the grid box average value.

A pressure gradient corresponding to geostrophical wind is used as a driving force in the simulation. The pressure gradient, the second term on the right hand side in Equation 3.8, is separated into a "basic state", i.e. the driving force, and a deviation from this "basic state" where $\bar{p}_r$ is the deviation:

$$\frac{1}{\rho_0}\frac{\partial \bar{p}_1}{\partial x_i} = f u_g \delta_{i2} - f v_g \delta_{i1} + \frac{1}{\rho_0}\frac{\partial \bar{p}_r}{\partial x_i} \tag{3.9}$$

where u_g and v_g is the geostrophic wind in the x and y direction and $f = 2\omega \sin\phi$. The first two terms on the right hand side represent the "basic state" and the last term the deviation from this.

The turbulent stress tensor is parameterized according to *K-theory*. It is assumed that the turbulent SGS stress, $\overline{u_i' u_j'}$, is coupled to the resolved field as,

$$\overline{u_i' u_j'} = -K_m \left(\frac{\partial \bar{u}_i}{\partial x_j} + \frac{\partial \bar{u}_j}{\partial x_i}\right) + \frac{2}{3}\bar{e}\delta_{ij} = (-2K_m S_{ij}) + \frac{2}{3}\bar{e}\delta_{ij} = \tau_{ij_{turb}} + \frac{2}{3}\bar{e}\delta_{ij} \tag{3.10}$$

where S is the strain tensor,

$$S_{ij} = \frac{1}{2}\left(\frac{\partial \bar{u}_i}{\partial x_j} + \frac{\partial \bar{u}_j}{\partial x_i}\right) \tag{3.11}$$

and $\bar{e} = \frac{\overline{u_i' u_i'}}{2}$ is the sub grid Turbulent Kinetic Energy, TKE. The elements on the diagonal of the matrix $\overline{u_i' u_j'}$ are written as $\overline{u_k' u_k'} = \overline{u_i'^2} = -2K_m \frac{\partial \bar{u}_k}{\partial x_k} + \frac{2}{3}\bar{e}$ (note no summation convention in this case, see Appendix II). K_m is the turbulent exchange coefficient. In the next chapter the SGS-model which task is to determine a good and representative K_m is described.

The TKE term, $-\frac{2}{3}\bar{e}$ is put together with the $\bar{p}_r$ term and inserted in Equation 3.8. The equations of motion can then be written in the way they are used inAndrén et al. [e.g. 1994] and Deardorff [1974] as well as in FOAM :

[1] $\overline{\bar{u}} = \bar{u}; \overline{u'} = 0; \overline{\bar{u}u'} = 0$; $\frac{\partial \bar{u}}{\partial x} = \frac{\partial \overline{u}}{\partial x}$ which is true for volume averaging. There are different ways to filter the equations and these averaging rules can not be applied to all filters.

$$\frac{\partial \bar{u}_i}{\partial t} + \frac{\partial \bar{u}_i \bar{u}_j}{\partial x_j} = [f u_g \delta_{i2} - f v_g \delta_{i1}] - \frac{\partial}{\partial x_i}\left(\frac{\bar{p}_r}{\rho_0} + \frac{2}{3}\bar{e}\right) - \frac{\partial \tau_{ij}}{\partial x_j} - 2\epsilon_{ijk}\bar{u_k}\Omega + \delta_{i3} g \frac{\bar{\theta} - \tilde{\theta}}{\theta_0} \tag{3.12}$$

Terms within brackets, [...], represent the "basic state" atmosphere. The stress tensor, τ_{ij}, is here defined with both a turbulent and a viscous part, $\tau_{ij} = \tau^b_{ij_{visc}} + \tau_{ij_{turb}}$, where $\tau^b_{ij_{visc}} = \frac{1}{\rho_0}\tau_{ij_{visc}}$ The viscous part is much smaller than the turbulent and may therefore be neglected, which is, however, not done in FOAM. $(\frac{\bar{p}_r}{\rho_0} + \frac{2}{3}\bar{e})$ is henceforth denoted $\bar{p}$.

3.2.1 Sub Grid Scale Model (SGS) The sub grid scale model used is a *one equation Eddy Viscosity Model* according to Moeng [1984]. In order to determine the turbulent viscosity coefficient, K_m, the SGS turbulent kinetic energy equation :

$$\frac{\partial \bar{e}}{\partial t} + \bar{u_j}\frac{\partial \bar{e}}{\partial x_j} = P + D + B - \varepsilon \tag{3.13}$$

is solved. From this prognostic equation the SGS turbulence energy $\bar{e}$ is used to calculate K_m. The terms on the right hand side in equation 3.13 represent shear production P, dispersion D, buoyancy production/reduction B and dissipation, ε:

$$P = -\overline{u_i' u_j'}\frac{\partial \bar{u}_i}{\partial x_j} = -\tau_{ij_{turb}} S_{ij} \tag{3.14}$$

$$D = \frac{\partial}{\partial x_j}\left(K_m \frac{\partial \bar{e}}{\partial x_j}\right) \tag{3.15}$$

$$B = \delta_{i3}\frac{g}{\theta_0}\overline{u_i'\theta'} = \delta_{i3}\frac{g}{\theta_0}\tau_{\theta i} \tag{3.16}$$

and

$$\varepsilon = C_\varepsilon \frac{\bar{e}^{\frac{2}{3}}}{l} \tag{3.17}$$

C_ε is empirical and set to 0.93 except at the lowest level where it is set to 3.9 due to wall effects as suggested by Deardorff [1980].

The SGS velocity stresses $\tau_{ij_{turb}}$ are assumed to be related to the resolved field by the turbulent exchange coefficient, K_m (see Equation 3.10) which, as a result of dimension analysis, may be written as a function of the SGS kinetic energy and a length scale, l, :

$$K_m = C_R l \sqrt{\bar{e}} \tag{3.18}$$

where $C_R = 0.1$. $l = \Delta s = (\Delta x \Delta y \Delta z)^{1/3}$ when $\frac{\partial \bar{\theta}}{\partial z} \leq 0$ and

$$l = l_s = 0.76 \cdot \bar{e}^{1/2} \cdot \left(\frac{g}{\theta_0}\frac{\partial \bar{\theta}}{\partial z}\right)^{-1/2} \tag{3.19}$$

when $\frac{\partial \bar{\theta}}{\partial z} > 0$ and $l_s < \Delta s$. This is a modification of l, suggested by Deardorff [1980], that takes into account the possible small mixing length in stable regions.

The heat flux in the SGS-model is assumed to have an analogous form,

$$\tau_{\theta i} = K_h \frac{\partial \bar{\theta}}{\partial x_i} \tag{3.20}$$

where the exchange coefficient for heat,K_h have the following relation to K_m:

$$K_h = \left(1 + (\frac{2l}{\Delta s})\right) K_m \tag{3.21}$$

The constants in Equation 3.17-3.19 are entirely empirical, Deardorff [1973, 1980]. The SGS-model should only describe the effects of the small eddies and if the resolution is high enough the empirical constants should not have much influence. However, close to the ground, where the eddies are small and therefore the SGS-model important, the LES is still dependent of the choice of SGS-model.

3.2.2 Differentiation Scheme When solving partial differential equations numerically, there are many methods for the discretisation i.e. how to calculate the derivatives necessary for solving the equations. The discretisation method is dependent on the grid structure of the domain. FOAM is constructed to handle unstructured arbitrary grids i.e. grids that can be used for a complex geometry. The domain is divided into cells which may have any general polyhedral shape as long as the cells are built of a number of flat faces and each face is shared with only one other cell or a boundary (the grid does not have to be constructed of orthogonal blocks). This means that the computational domain in FOAM may have quite a complex geometry. In this study however, a simple geometry with orthogonal blocks is used.

The discretisation used is called *Finite Volume Discretisation*, a scheme that can be used for complex structures. Each point where differential equations is solved, is situated in the center a cell. All variables are defined in these points which means that FOAM works with unstaggered grid, although staggered grids are often used in other LES.

3.2.3 Finite Volume Discretisation When discretising the equations, it is important to have the same order of accuracy in the numerical scheme as well as for the sub grid model. FOAM uses the integral form of the partial differential equations in its discretisation scheme. The integral form of the momentum equation, Equation 3.12 can be written as:

$$\int_t^{t+\Delta t} \left[\int_V \frac{\partial \bar{u_i}}{\partial t} dV + \int_V \frac{\partial \bar{u_i}\bar{u_j}}{\partial x_j} dV \right] dt = \int_t^{t+\Delta t} \left[-\int_V \frac{\partial}{\partial x_i} \left(\frac{\bar{p}_r}{\rho_0} + \frac{2}{3}\bar{e} \right) dV - \int_V \frac{\partial \tau_{ij}}{\partial x_j} dV + \int_V \mathbf{X} dV \right] dt \tag{3.22}$$

where V is the volume of the cell, Δt the time step and $\mathbf{X}$ the terms without derivatives. By using the Gauss' theorem the volume integrals are transformed into surface integrals. They may be calculated as the sum of the integrals of each face of the cell. The advection term in Equation 3.22, the second term on the left hand side become:

$$\int_V \frac{\partial \bar{u_i}\bar{u_j}}{\partial x_i} dV = \sum_{faces} S_f^i (\bar{u_i}\bar{u_j})_f = \sum_{faces} (S_f^i(\bar{u_i}))\bar{u_j}_f = \sum_{faces} F\bar{u_j}_f \tag{3.23}$$

The index f denote the center of the cell *faces*. F is the face flux $F = S_f^i(u_i)_f$ where S is the cell surface area. The face flux is used for the U equation as well for the θ equation in the numerical scheme which is computationally efficient.

The face flux is calculated iteratively while balancing the pressure and velocity field. The value of $\bar{u_j}_f$ ($\bar{\theta}_f$ in the theta equation) is calculated through central differencing, using the value of $\bar{u_j}_c$ in the cells on each side of the cell face. Central differencing has second order of accuracy. The pressure term in Equation 3.22, the first term on the right hand side, is discretised with central differencing too, but there is no the face flux involved.

The stress term has second derivatives which are discretised in a similar way as above. The Gauss' theorem transforms it into a sum over the cell faces. On the cell faces the derivative is calculated trough the difference between the values in the cell centers on each side of the face, divided with the distance. This is also of second order of accuracy.

The time derivative, the first term in Equation 3.22 has a few different discretisation schemes predefined in the FOAM C++ library. We use *Backwards Differencing* which is a second order accurate scheme. It uses three time steps, $t, t-\Delta t, t-2\Delta t$ and gives the following expression for the derivative (see Jasak [1995]):

$$\frac{\frac{3}{2}u_i^{(t)} - 2u_i^{(t-\Delta t)} + \frac{1}{2}u_i^{(t-2\Delta t)}}{\Delta t} \tag{3.24}$$

We can now put the whole discretised momentum equation together:

$$\frac{\frac{3}{2}u_i^{(t)} - 2u_i^{(t-\Delta t)} + \frac{1}{2}u_i^{(t-2\Delta t)}}{\Delta t} V + \sum_{faces} F u_i = -\sum_{faces} S_f^i \left(\frac{\bar{p}_r}{\rho_0} + \frac{2}{3}\bar{e} \right) - \sum_{faces} S_f^i \tau_{ij} + X \tag{3.25}$$

where V is the volume of the cell. For the temperature equation the discretisation procedure is done in a similar way. The FOAM system is much more complex than this, but the overall picture has been explained. The problem with unstructured grids has not been looked into but since the simulations made has a simple grid structure that is of minor interest here. Still it's necessary to point out why FOAM is built in this way.

4. The Numerical Experiments

The planetary boundary layer has not been simulated with FOAM earlier. Changes from previous FOAM codes are

- The Coriolis force has been implemented in the equations.
- The effect of the buoyancy has been implemented in the equations (both in the momentum equation and the SGS TKE equation).
- The domain and grid boxes are larger since the simulated turbulent scales are larger Previously has only flows with turbulent scales much smaller than in the PBL been simulated.
- An aerodynamically rough surface is modelled. Previously has the friction against walls been a function of the laminar viscosity only and not of the turbulence (aerodynamically smooth walls).

The neutral, stable and unstable boundary layer has been simulated in order to validate FOAM. For the stable atmosphere two experiments with different domains was made.

When setting up the flow, FOAM was first run with a constant forcing (the pressure gradient corresponding to geostrophical wind) and neutral stratification. Initially a flow far from steady state was used. After 30 hours a well developed boundary layer, statistically close to a steady state, was developed. From this state started the validation experiments.

4.1 Grid and Boundary Conditions

FOAM was set up to resemble the LES codes used for comparison. A domain with simple geometry, where all grid boxes had the same size, was set up. Numerical and external parameters for the different runs are presented in Table4.1. The total domain was $4000 \times 2000 \times 1500$ meter in x,y and z direction. It had 40 grid boxes in each direction. This is the same grid Andrén et al. [1994] used for neutral PBL simulations. The grid is not a computationally expensive grid, which was necessary because of the time available and the access to computer power for the FOAM tests. One way to validate a LES code is to compare it with "better simulations", e.g. simulations with higher resolution which is the case for the stable PBL. The resolution in the domain had to be changed for the stable atmosphere. With the same number of grid boxes and a domain size of $2000 \times 1000 \times 750$ meter a new simulation was done.

The domain was situated at latitude 45°north and the flow was driven with a constant pressure gradient. The driving force of the system, the pressure gradient, was chosen to correspond to a geostrophic wind with different magnitude for each case, see Table 4.1.

In FOAM there is a number of different predefined boundary conditions, e.g. "fixed value" or "zero gradient". When a "fixed value" is set as boundary condition that value is used throughout the whole simulation. "Zero gradient" gives the boundary the same value as in the cell center. Cyclic boundary conditions is used at the four vertical walls of the domain while the top and bottom boundaries is treated different for different variables, displayed in Table 4.2.

"Zero gradient" is used for $\bar{\theta}$ at the top and the bottom and for the turbulent kinetic energy at the bottom. For the winds at the top boundary "zero gradient" was used for U and V while W had "fixed value" (= 0) giving a stress free boundary

[1] The 60^3 and 80^3 grids are discussed in chapter 4.4

Case	Domain size $x \times y \times z$ (meter)	$N_x \times N_y \times N_z$	Surface Heat Flux (K m·s^{-1})	u_g (m·s^{-1})
Neutral 1	$4000 \times 2000 \times 1500$	$40 \times 40 \times 40$	0	10
Neutral 2 [1]	$4000 \times 2000 \times 1500$	$60 \times 60 \times 60$	0	10
Neutral 3	$4000 \times 2000 \times 1500$	$80 \times 80 \times 80$	0	10
Unstable	$4000 \times 2000 \times 1500$	$40 \times 40 \times 40$	0.02	15
(Stable 1)	$4000 \times 2000 \times 1500$	$40 \times 40 \times 40$	-0.005	7
Stable 2	$2000 \times 1000 \times 750$	$40 \times 40 \times 40$	-0.005	7

Table 4.1: Numerical and external parameters in the simulated cases

condition. At the bottom wall all the winds were set to zero. The pressure was set to zero at the top and to "zero gradient" at the bottom. Note that the hydrostatic

Variable	Bottom Wall	Top Wall
$\bar{U}$	0	$\frac{\partial \bar{u}}{\partial z} = \frac{\partial \bar{v}}{\partial z} = 0; \bar{w} = 0$
$\bar{e}$	0	$\frac{\partial \bar{e}}{\partial z} = 0$
$\bar{p}$	$\frac{\partial \bar{p}}{\partial z} = 0$	0
$\bar{\theta}$	$\frac{\partial \bar{\theta}}{\partial z} = 0$	$\frac{\partial \bar{\theta}}{\partial z} = 0$

Table 4.2: Boundary Conditions

balance is implemented in the equations and that $\bar{p} = \frac{\bar{p}_r}{\rho_0} + \frac{2}{3}\bar{e}$. At the lower boundary a momentum sink, τ_{ij_0}, is introduced, i.e. the momentum flux "across" the boundary:

$$\tau_{13_0} = -C_D \tilde{\tilde{\mathbf{U}}} \cdot \bar{u_1} \tag{4.1}$$

$$\tau_{23_0} = -C_D \tilde{\tilde{\mathbf{U}}} \cdot \bar{u_2} \tag{4.2}$$

where index 0 represent the lower boundary and $\tilde{\tilde{\mathbf{U}}} = \sqrt{\tilde{\bar{u}}_1^2 + \tilde{\bar{u}}_2^2}$ is the time average of the horizontal wind. C_D is the drag coefficient:

$$C_D = \kappa^2 \left(\ln z/z_0 - \Psi(z/L) \right)^{-2} \tag{4.3}$$

where $\Psi = 0$ for neutral stratification [see Arya, 1988, section 11.4]. This was unfortunately used for all simulations, since the calculation ofC_D was set up for the neutral case and was not changed for the unstable and stable simulations. The principal result is that a different effective z_0 was used in the simulations. A similar method is used for the heat flux.

4.2 The Neutral Case

The first test was for the *neutral* boundary layer. A completely neutral PBL with constant temperature in the domain was used. This caused the buoyancy term in the equation of motion and the total temperature equation to be passive in this experiment.

The same resolution, grid structure and initial parameters as Andrén et al. [1994] (henceforth referred to as Andrén94) was used to make the comparison easy to perform. Starting from the flow at the end of the 30 hour simulation, FOAM was run for 6+3 hours to find a steady state. Statistics was sampled during the three final hours. The forcing in the simulation is a pressure gradient in the y-direction corresponding to a geostrophic wind, $u_g = 10\text{m}\cdot\text{s}^{-1}$.

4.2.1 Results The friction velocity for the neutral simulations are shown in Table 4.3, the FOAM value compared to the span of results from the simulations by Andrén94. The FOAM result lies within the results from Andrén94.

Models	u_* (m·s^{-1})	z_0 (m)
FOAM	0.407	0.1
Andrén94	0.402-0.448	0.1

Table 4.3: Parameters for the *neutral case*. Friction velocity, u_* and roughness parameter, z_0.

In Figure 4.1 the mean wind characteristics are shown, u-wind, v-wind, total horizontal wind and the horizontal wind direction (this is not presented in Andrén94). All figures in this paper shows *horizontal averages* of the variables. An increase of the horizontal wind with height can be seen. Closer to the ground friction slows down and changes the direction of the wind (i.e an Ekman spiral is created, Holton [e.g. 1992, section 5.3.4]). The wind is close to geostrophic between 800 meter and the top of the domain while it reaches zero at ground level. There is a 14°change of the wind direction through the domain. At high altitudes the wind is slightly super geostrophic, 10.5 m·s^{-1}, and the wind flows towards lower pressure. This deviation from geostrophic flow could indicate that there still is a small reminiscence of an inertial oscillation; the LES has not yet reached it's steady state.

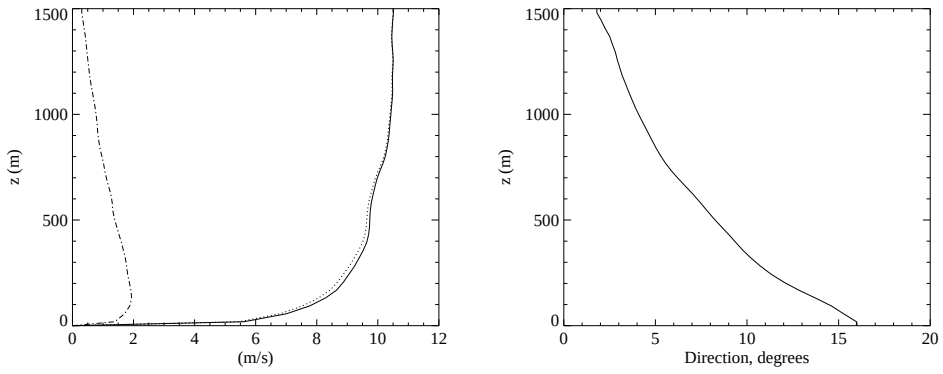

Figure 4.1: The *neutral case* (horizontal averages). Winds for FOAM, right figure, horizontal wind (full line), U-wind (dotted) and V-wind (dash-dotted). Horizontal wind direction for FOAM, left figure.

The Monin-Obukhovs similarity function, Φ_m, [e.g. Arya, 1988, chap. 11.1] is plotted in Figure 4.2. $\Phi_m = \frac{\kappa z}{u_*}\frac{\partial |\mathbf{U}|}{\partial z}$ where κ is the von Karman constant, u_* the friction velocity and $\mathbf{U}$ the horizontal velocity vector. Andrén94 compared different LES to determine the importance of the SGS-models and the numerical methods for the neutral boundary layer. Their result for different simulations are shown to the right in Figure 4.2 while the FOAM result is to the left.

Regarding Φ_m, Figure 4.2 where Φ_m is plotted as a function of normalized height [2], the FOAM result lies within the span of Andrén94s results. Φ_m should, according to the similarity theory, be constant (= 1) in the logarithmic surface layer in a neutral flow. Compared to Andrén94, only their SGS-model with backscatter managed to recreate that to an acceptable degree. A backscatter model, which is rather computer expensive, scatter kinetic energy back to larger scales from smaller, opposite the

[2] $h = 0.35\frac{u_*}{f}$ is often used for determining the neutral PBL height i.e. the PBL-height is at $\frac{z \cdot f}{u_*} = 0.35$.

direction of the energy cascade. Compared to the other models in their experiment FOAM produced a very similar result, an increase in Φ_m or wind shear a little bit above ground. This is a well known problem for LES. Sullivan et al. [1994] has proposed a SGS-model which eliminates this problem, however, this model relies heavily on the concept of horizontal homogeneity which is of no use to FOAM since a future aim is to use FOAM for simulations with horizontal inhomogeneities. Still FOAM has a somewhat weaker Φ_m maxima than most of the LES tested by Andrén94 which is a good indication of FOAM behavior.

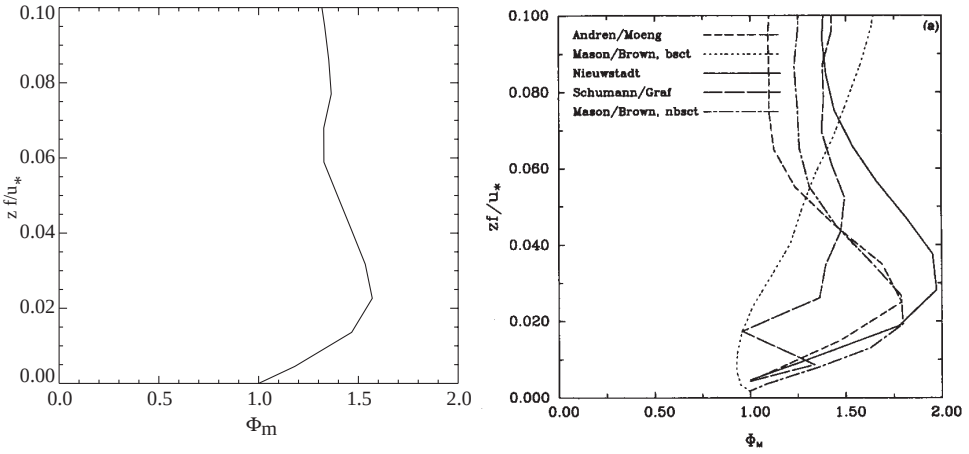

Figure 4.2: The *neutral case* (horizontal averages). Monin-Obukhovs similarity function, Φ_m in the lower part of the PBL. FOAM to the left and Andrén94 to the right.

A second moment is in the presentation denoted by e.g. $\overline{uw}$ which is the horizontal average of the sum of the resolved scale part and the SGS part. The resolved scale part is calculated as: $< \bar{u}''\bar{w}'' >=< (\bar{u} - < \bar{u} >)(\bar{w} - < \bar{w} >) >$, where <> denotes time averages. In the figures horizontal averages of the second moments and their components are plotted. The same notation is used for the wind variances e.g. $\overline{u^2}$. Note that in the case of second moments ($^-$) does not denote volume averages.

In Figure 4.3 the normalized variances for the wind component, $\overline{u^2}/u_*$, $\overline{v^2}/u_*$ and $\overline{w^2}/u_*$, are plotted as functions of the normalized height. The sub grid part and the total variances are plotted for FOAM and Andrén94. In the result from FOAM also the resolved part is plotted. The FOAM results are plotted to the left and Andrén94's result to the right. FOAM show similar result as Andrén94. FOAM have the same magnitude for the maxima as for some of the codes in Andrén94 in all variances, both for the total and SGS part. In the total $\overline{u^2}/u_*$ the maxima for Addrén94 lies higher up in the domain then in FOAM. In all the variances a small but systematic deviation between the FOAM and the Andrén94 results can be seen. The total variances are slightly less for FOAM than for Andrén94, i.e. FOAM generates a little bit less turbulence than Andrén94. Since this is a neutral simulation all turbulence is shear generated.

The influence of the SGS model is large close to the ground, especially at the first grid point above ground. This is very clear for $\overline{v^2}/u_*$ and $\overline{w^2}/u_*$ where FOAM and Andrén94 show similar results.

High up at the top of the plotted domain we see some irregularities, clearest in $\overline{w^2}/u_*$. This could be due to our top boundary condition for $\bar{p}$, where $\bar{p}$ is set to zero. However, since it does not seem to interfere with the lower parts of the the domain this problem is left for later studies. In Figure 4.4 normalized momentum fluxes $\overline{uv}/u_*$ and $\overline{uw}/u_*$ are shown. The same irregularities in the top of the FOAM domain, as in the wind variances, can here be seen. The momentum fluxes, $\overline{vw}/u_*$ show a somewhat smaller maxima compared to Andrén94, otherwise the magnitudes

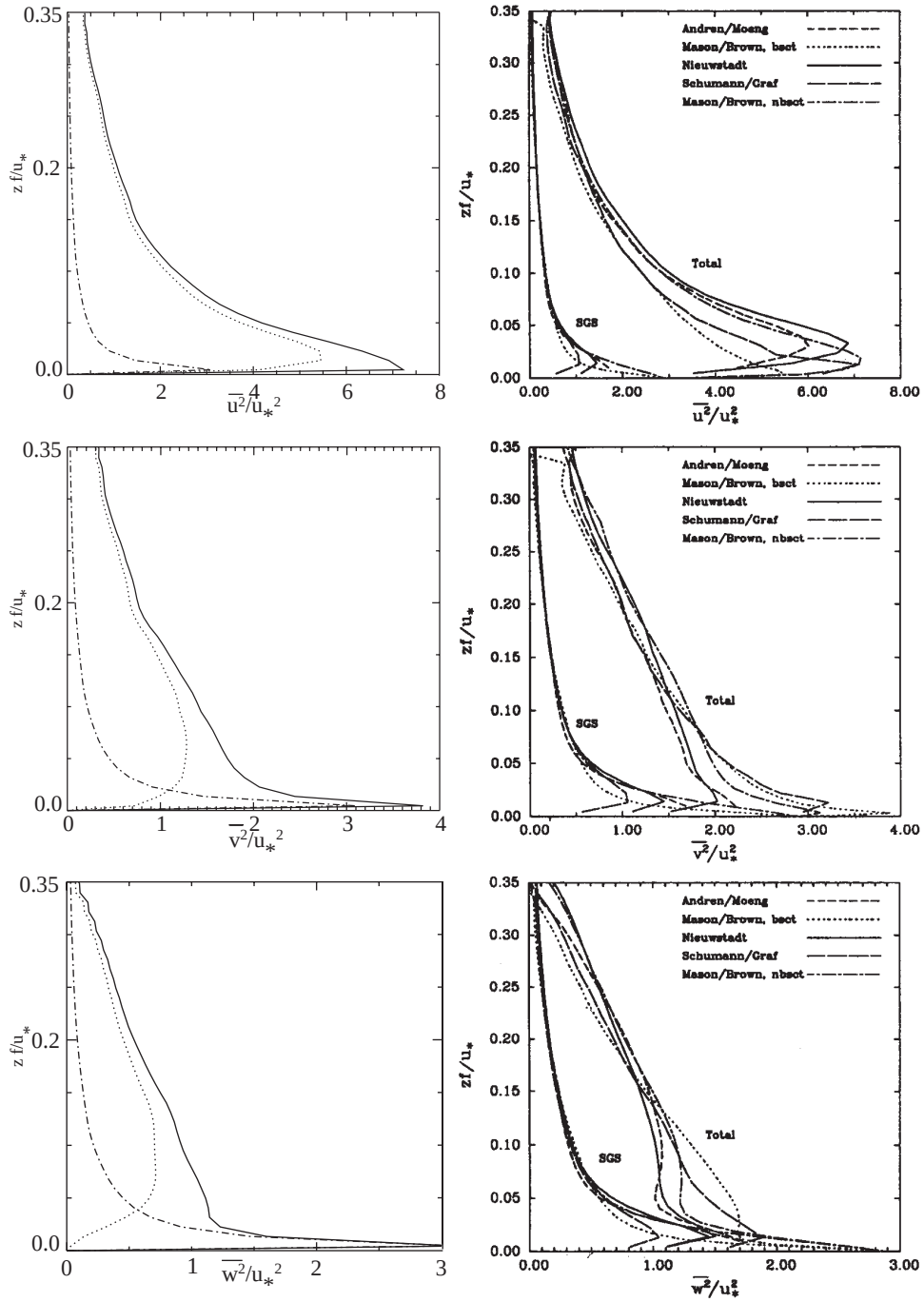

Figure 4.3: The *neutral case* (horizontal averages). Normalized velocity variances for the FOAM results showing: total variance (solid), resolved part (dashed) and SGS part (dash-dotted), left figures. Total and SGS part from Andrén94, right figures (the resolved part is not presented in the results from Andrén94).

and characteristics are the same. The overall correspondence with the results from Andrén94 is rather good.

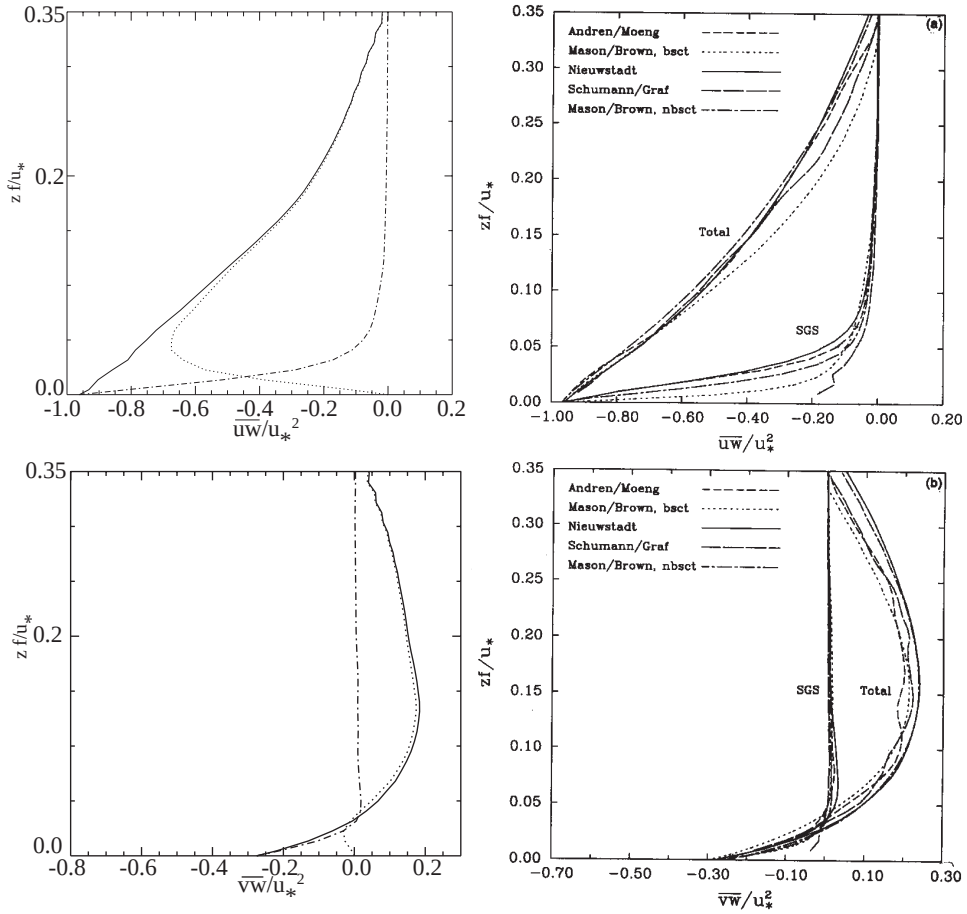

Figure 4.4: The *neutral case* (horizontal averages). Normalized momentum fluxes: total variance (solid), resolved part (dashed) and SGS part (dash-dotted) for FOAM, left figures. Total and SGS part for Andrén94, right figures (the resolved part is not presented in the results from Andrén94).

4.3 The Unstable Case

A simulation with an *unstable* PBL was performed, a first test to see if FOAM could transform the neutral PBL into an unstable. The same grid as for the neutral case was used, assuming that the larger turbulent scales in a convective PBL would be sufficiently resolved. The flow at the 6th hour of the neutral case was used as starting field to see that the buoyancy and thermodynamic equation works in the "right direction". To change the stability in the neutral PBL, heat was added at ground level (with aid of a source term in the temperature equation). Through the experiment, 0.02 K m·s^{-1}(20.08 Wm^{-2}) was constantly added at the first vertical level. This raised the temperature at the bottom of the domain and turbulent transport distributed it upwards. The chosen temperature flux is rather weak for an unstable PBL but it was a first step in validating FOAM for the unstable PBL.

The driving force was increased to match a geostrophic wind at 15ms^{-1}instead of 10m·s^{-1}with the purpose to resemble a previously made experiment for the unstable PBL, Sullivan et al. [1994]. Unfortunately the results from that experiment turned out to be rather poorly documented which made comparisons difficult.

Many experiments with the unstable PBL have a strong inversion aloft in the domain to limit the growth of the PBL. This FOAM simulation lack this inversion which lets the unstable PBL grow through the whole domain and the PBL height is limited only by the size of the domain. For these reasons only the change of the PBL from neutral to unstable will be discussed here. More careful experiments are left for future work.

The driving pressure gradient was changed anyhow which also the winds in the starting field were. All winds at the 6th hour of the neutral run was multiplied with 1.5 to give a wind field closer to the expected steady state. From this point a simulation 6+3 hours long was made, the last three hours used for calculating statistics.

4.3.1 Results The wind field in terms of u-wind, v-wind and horizontal wind is plotted to the left in Figure 4.5 together with the horizontal wind direction, i.e. the deviation in degrees from the direction of the u-wind.

There are small variations of the horizontal wind with height apart from the lowest 100 meter. These features, a mixed layer above the surface layer, are typical for the unstable boundary layer. Compare with the starting field for this simulation, i.e. the neutral simulation, the wind properties shown in Figure4.1 (note that all winds here have been multiplied with 1.5 for the starting field in the unstable simulation).

The angular change of the horizontal wind through the domain is also much less in the convective simulation than in the neutral, which also is a feature that should be expected, from a wind change vertically through the domain of 14°to 2°. However, the wind is not geostrophic, it is still blowing towards lower pressure demonstrating that the profile still is far from a steady state.

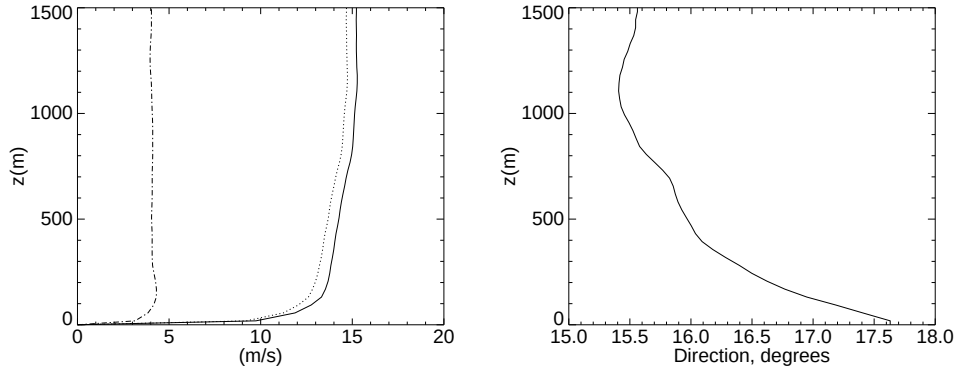

Figure 4.5: The *unstable case* (horizontal averages). Horizontal wind (solid), U wind (dotted) and V wind (dash-dotted) for FOAM (left figure). Horizontal wind direction for FOAM (right figure).

The temperature profile for the unstable PBL is shown in Figure4.6 together with the normalized temperature flux, $\overline{w\theta}/\overline{w\theta}_0$ where $\overline{w\theta}_0$ is the temperature flux at the ground level, 0.02 K m·s^{-1}in this simulation. Through the PBL the temperature flux decreases constantly with height. The temperature profile shows large gradients in the surface layer to become smaller in the "mixed layer" above 100-200 meter i.e. turbulent mixing in the "well mixed" layer is almost effective enough to cause a constant value.

The Monin Obukhov similarity function, Φ_m, is plotted in Figure 4.7. Φ_m is a normalized shear that should be much less in the unstable case than in the neutral. The FOAM result is the solid line and dashed line is the theoretical value for similarity theory in the unstable PBL [e.g. Arya, 1988, chapter 11.2]. Compared to Φ_m in the neutral FOAM case the unstable simulation has changed Φ_m to have unstable

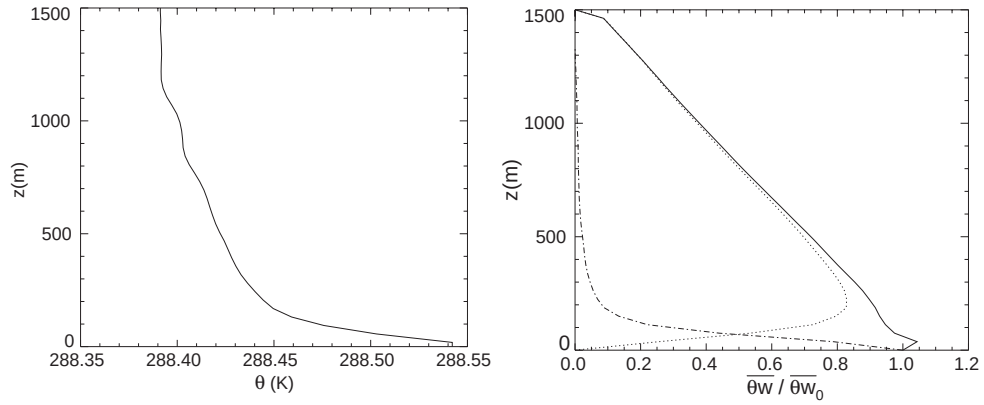

Figure 4.6: The *unstable case* (horizontal averages). Potential temperature, θ, for FOAM (left) and normalized temperature flux $\overline{w\theta}/\overline{w\theta}_0$, for FOAM (right).

characteristics. The maximum close to ground in the neutral case, Figure4.2, is only visible at the lowest level. Although the resulting Φ_m deviates from the theoretical one, it clearly demonstrates that the influence of the buoyancy term is working in the "right direction".

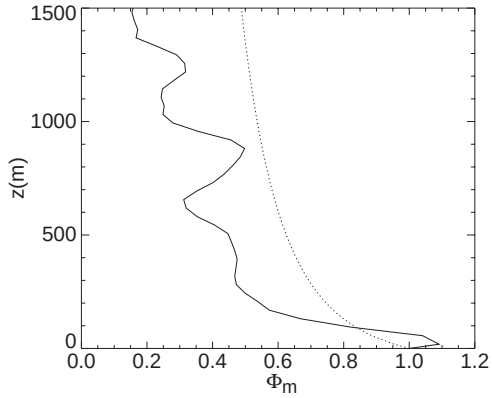

Figure 4.7: The *unstable case* (horizontal averages). Monin-Obukhov Similarity Function, Φ_m, FOAM (solid), theoretical value (dashed).

The normalized momentum fluxes $\overline{uw}/u_*$ and $\overline{vw}/u_*$ for the unstable simulation are shown in Figure 4.8. The total flux, resolved part and SGS part are plotted. In the convective PBL the SGS model should have much less influence than in the neutral and stable PBL. There is a small jump in the total momentum flux for $\overline{uw}/u_*$ where the resolved part looses influence and the SGS part takes over. Compared to the neutral simulation there are no positive values in $\overline{vw}/u_*$, which is a result of that the v-wind no longer decreases with altitude.

In the wind-variances the differences between SGS and resolved scales can be seen even clearer. Total, SGS and resolved part of the normalized variances $\overline{u^2}/u_*$, $\overline{v^2}/u_*$ and $\overline{w^2}/u_*$ is plotted in Figure 4.9. The SGS part seems to have reasonable influence in the variance for $\overline{u^2}/u_*$ while it seems like the SGS influence is to large in $\overline{v^2}/u_*$, and even more so in $\overline{w^2}/u_*$. This was also somewhat detected in Figure4.3 in the neutral case. It is, however, difficult to determine if this is an effect due to lack of balance in the field or because of the SGS-model, which is a topic for further investigations.

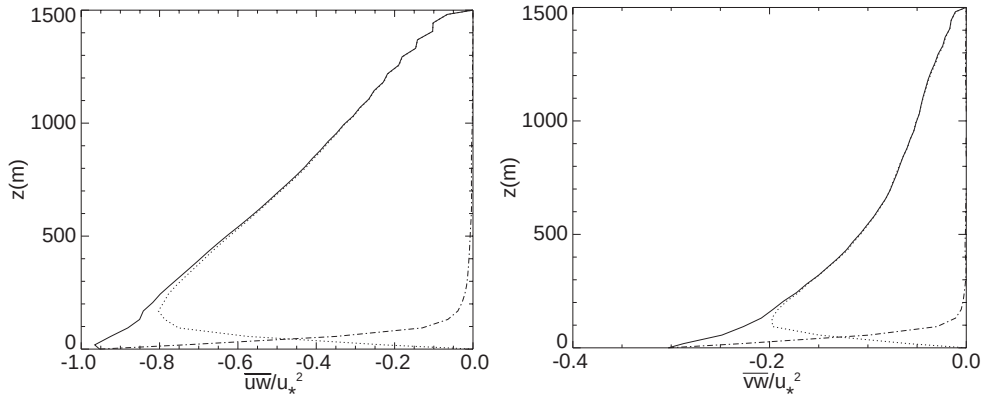

Figure 4.8: The *unstable case* (horizontal averages). Normalized momentum fluxes for FOAM, $\overline{uw}/u_*$ (left) and $\overline{vw}/u_*$ (right). Total flux (solid), resolved contribution (dotted), SGS contribution (dash-dotted)

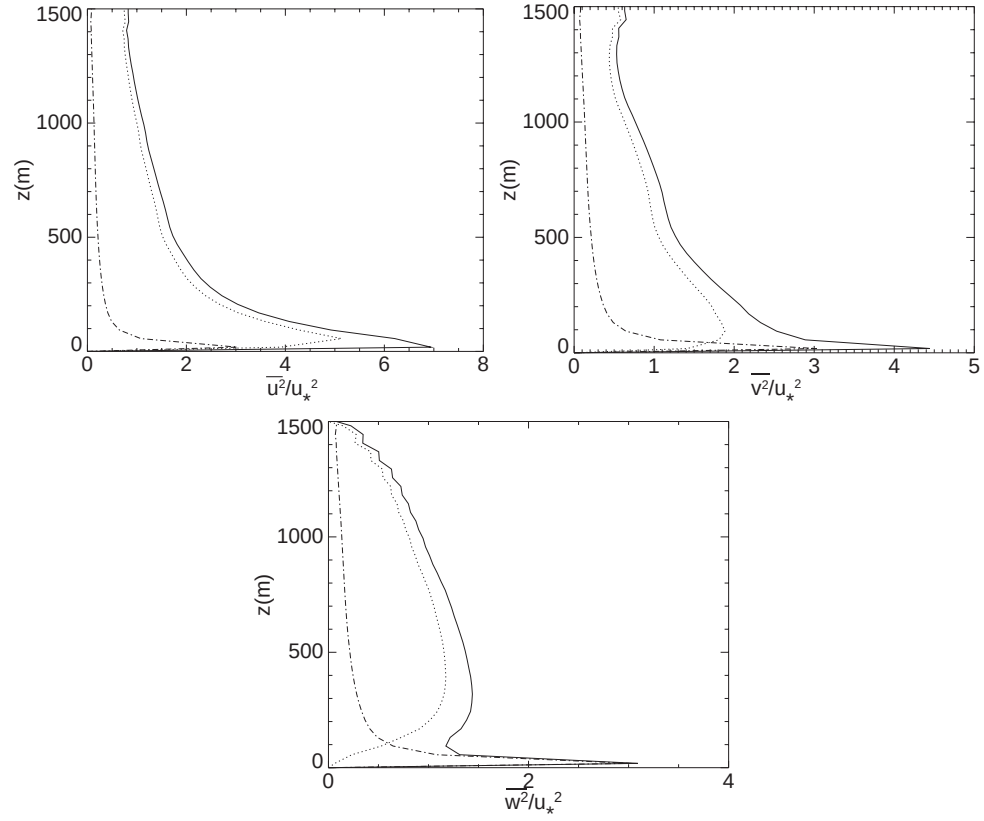

Figure 4.9: The *unstable case* (horizontal averages). Normalized wind correlations for FOAM, $\overline{u^2}/u_*$, $\overline{v^2}/u_*$ and $\overline{w^2}/u_*$. Total correlation (solid), Resolved contribution (dotted), SGS contribution (dash-dotted).

4.3.2 The Stable Case The experiment with a *stable* PBL started from the 6th hour of the neutral run. Also in this case the driving force was changed. The pressure gradient in the y-direction that correspond to a geostrophical wind was decreased from $10\text{m}\cdot\text{s}^{-1}$to $7\text{m}\cdot\text{s}^{-1}$, in order to resemble the conditions in Andrén [1995], henceforth referred to as Andrén95. To speed up the geostrophic adjustment, all wind speeds

Model	z_0	u_* (m·s^{-1})	θ_*(K)	L(m)	h(m)
FOAM	0,13	0,232	0,0215	184	340
Andrén95	0,10	0,231	0,0216	178	285

Table 4.4: Internal parameters of the simulated *stable* PBL for FOAM and Andrén [1995]

in the starting field was multiplied with 0.7 [3]. The stability in the neutral flow was changed with a constant cooling at the ground. $0.005K/s$ ($= 5.02W/m^2$) was constantly removed during the simulation. A 6+3 our run was made, the last three for sampling statistics.

The same grid structure as in the neutral simulation was first used which turned out to be unfortunate. Close to the ground obvious errors were visible, probably because of the poor resolution. A stable PBL simulation requires higher resolution than a neutral or unstable simulation. Due to the fact that the stable atmosphere suppress the large scale turbulence and more of the energy in the PBL is located in smaller eddies, as a result of the energy cascade, higher resolution is needed or the SGS-model gets too much influence.

The grid structure was changed compared to the first experiment. The resolution was increased by dividing all the distances in the grid with with a factor 2. It is still a coarse grid for stable boundary layer simulations but available computer power had to be taken into consideration. The result was compared with other experiments with the stable atmosphere performed by Andrén95. Andrén95 uses a higher resolution than FOAM, $96 \times 96 \times 96$ grid points, where the domain had the size of $600 \times 400 \times 500$ meters in x, y and z direction respectively. The resolution for FOAM in the stable case is much less, (Table 4.1), but hopefully sufficient enough to give a hint whether the buoyancy force is working in the "right direction".

4.3.3 Results In Table 4.4 parameters of the planetary boundary layer can be compared for FOAM and Andrén95. FOAM used a z_0 that was a little bit larger than what Andrén95 used, due to the mistake of using the same stability in the code for the neutral as for the stable (and unstable) case in calculating the drag coefficient, C_D. The value in table is corrected for this effect.

The parameters u_* and θ_* was almost the same for FOAM and Andrén95. The surface layer parameters in FOAM seems to correlate with Andrén95. The Monin-Obukhov length, L was slightly larger for FOAM and the PBL-height, h, was 50 meter higher. The PBL-height was calculated as the height where the temperature flux was reduced to 5% of its surface value, as in Andrén95. It should be noted that the variation of the temperature flux was highly irregular at the PBL height, so the value is not very well determined. Compared to the initial neutral profile, FOAM decreased the PBL-height because of the buoyancy damping of turbulence. With a lower PBL-height and a lower Monin-Obukhov length, the simulation by Andrén95 managed to suppress the turbulence even more than FOAM. There will be a longer simulation with FOAM to see if these discrepancies disappear when a steady state is reached.

Figure 4.10 shows the horizontal wind and wind direction. There is a low level jet with a maximum of 8 m·s^{-1}at the PBL-height. Above the jet a slightly super geostrophic wind can be seen, 7.4 m·s^{-1}. The change of wind direction with altitude has increased, as expected compared to the neutral case. In the stable case there is even a flow towards *higher* pressure at the top and the wind direction changes around 38 degrees through the domain. At the bottom the wind blows towards lower pressure. The pressure gradient has not yet balanced the coriolis force. The inertial oscillation

[3] In the neutral case there was a geostrophical wind at 10ms^{-1}and a geostrophical wind at 7m·s^{-1}was expected in the stable case

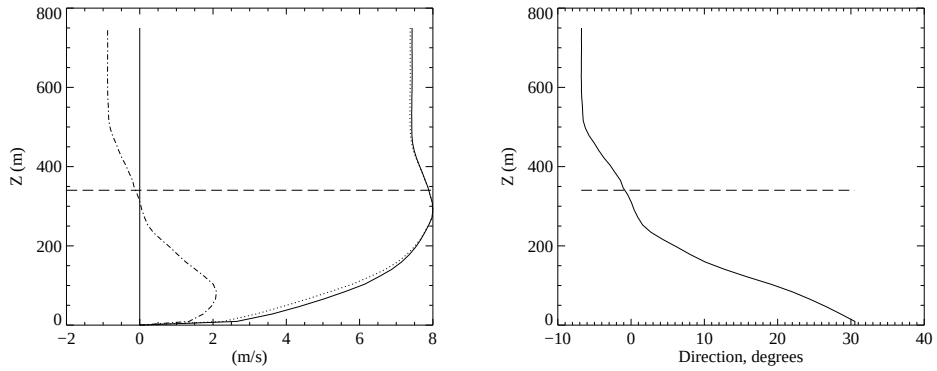

Figure 4.10: The *stable case* (horizontal averages). Horizontal wind (solid), U wind (dotted) and V wind (dash-dotted) for FOAM (left figure). Horizontal wind direction for FOAM (right figure). The dashed line is the PBL-height.

is much lager here than in the neutral case, as expected, and the flow is far from a steady state.

The temperature profile at the end of the run is plotted to the left in Figure4.11. Only about 0.8 K difference through the domain is seen in the FOAM result which makes the PBL weakly stable. It is not enough for a validation of the stable PBL, a much longer simulation must be made to find a steady state. Still it is obvious enough to, via the buoyancy effects, drastically alter the flow towards a stable stratification state. Unfortunately there is no temperature profile in the article by Andrén95 to compare with. Worth noticing is that the tendency for the temperature change with height is increasing at about 100 meter while it's decreasing at 200 meter which seems somewhat peculiar. It could be explained by the lack of balance in the flow.

The Monin-Obukhov similarity function is potted to the right in Figure 4.11, together with the theoretical value for a stable PBL [seeArya, 1988, section 11.2]. In the layer below $0.4\,z/h$ FOAM correlates with the similarity theory for a stable PBL. This is a region where it seems like a stable PBL is created. Above this level, high levels of turbulence persists (Figure 4.14) possibly fossil turbulence from the neutral initial conditions. Although the simulated profile has too large values in the surface layer, the difference from the neutral case is in accordance with the theory.

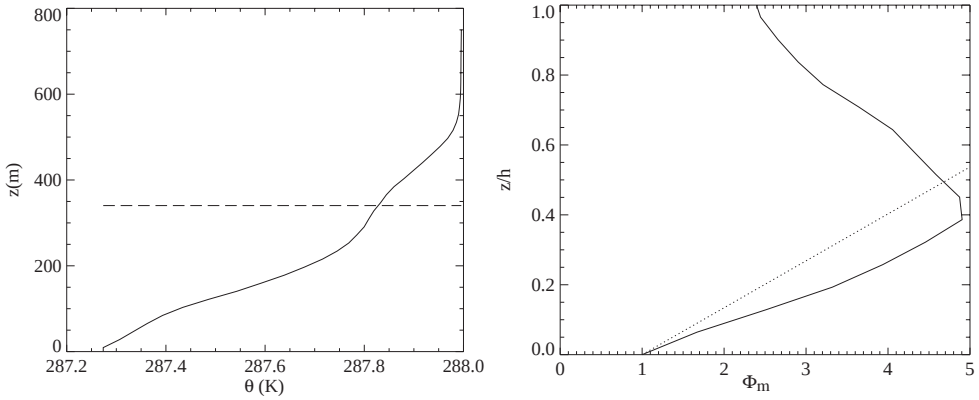

Figure 4.11: The *stable case* (horizontal averages). The potential temperature θ for FOAM (left figure). The dashed line is the PBL-height. The Monin Obukhov similarity function, Φ_m (right figure). FOAM value (solid), theoretical value for the stable PBL (dotted).

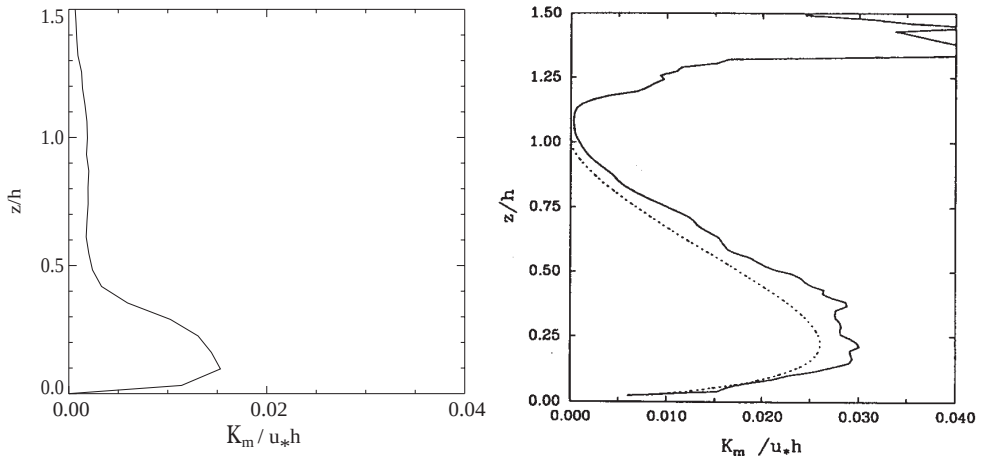

Figure 4.12: The *stable case* (horizontal averages). Eddy viscosity coefficient, K_m. FOAM, left figure and Andrén95, right figure.

If we compare the SGS eddy viscosity coefficient for our case K_m with Andrén95, Figure 4.12, they show a similar pattern. There is a maxima at about the same height but for FOAM it is much weaker. Note that the normalization of K_m is made with the PBL height, h, on both axes in the plot. If the PBL height would be set e.g. where the similarity function, Φ_m, has its maximum, $z/h \approx 0.4$ in Figure 4.11, the appearance of K_m would be very similar for FOAM and Andrén94. A weaker K_m means less SGS fluxes and less SGS TKE but it is difficult to draw conclusions from the values here.

Andrén95 made two experiments for this stable PBL. In the first a neutral layer was situated aloft in the flow, which will be used for comparison with FOAM, and in the second a finite stratification was used aloft. When looking upon the potential temperature, $\bar{\theta}$, for the stable FOAM run, Figure 4.11, a neutral layer at around 550 meter and up should be seen. The Brunt-Vaisala frequency is plotted in Figure 4.13 for FOAM and for Andrén95. In Andrén95's figure the solid line is the run with a neutral layer aloft that can be compared with FOAM. At $z/h = 1.5$ both simulations have a similar value which increases towards lower altitude. FOAM and Andrén95 have a similar value at $z/h = 0.5$ but Andrén95 has a constant Brunt-Vaisala frequency below the PBL-height where FOAM still increases towards ground. Close to the ground there are completely different tendencies. Andrén95's LES has an increase in the Brunt-Vaisala frequency while there is a decreases in FOAM. It is the same pattern that could be seen in the tendency of the potential temperature (N is a function of $\frac{\partial \theta}{\partial z}$). It would be interesting to see if this feature still would remain when the FOAM simulation reaches a steady state.

The normalized wind variances, $\overline{u^2}/u_*$, $\overline{v^2}/u_*$ and $\overline{w^2}/u_*$, plotted in Figure 4.14 does only have some equalities between the simulations made by FOAM and Andrén95 and that is close to the ground. The maximum for the variance $\overline{u^2}/u_*$ is similar here and the variances for $\overline{v^2}/u_*$ and $\overline{w^2}/u_*$ is slightly larger for FOAM. The SGS part (which in FOAM is the same for all variances) is much larger in FOAM. This is due to that FOAM uses a courser resolution which gives the SGS-model much more influence. Higher up in the flow FOAM shows completely different results than to Andrén95. This is probably a consequence of the fact that the FOAM simulation is far from its equilibrium state.

There are differences between FOAM and Andrén95 in the momentum fluxes, Figure 4.15, which could also be due to the resolution. The normalized total horizontal flux, denoted as τ in the figure, is larger than one up to $0.2z/h$ due to the SGS part,

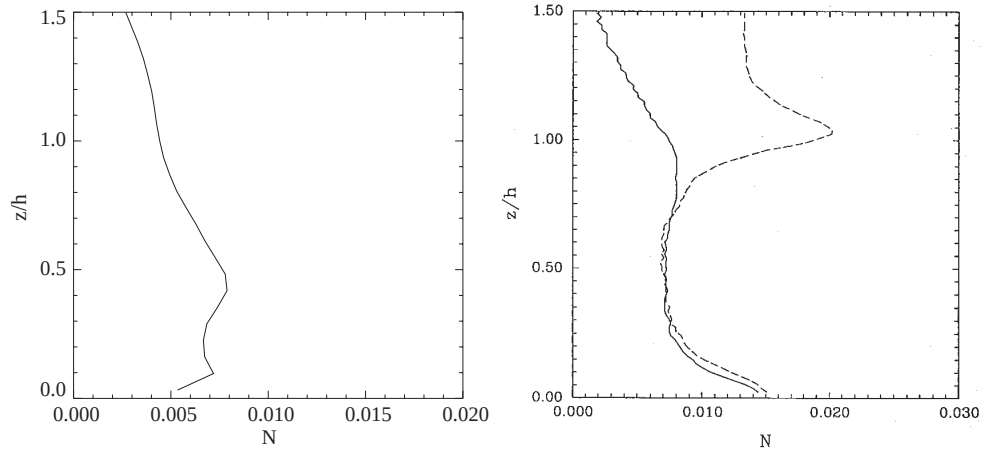

Figure 4.13: The *stable case* (horizontal averages). The Brunt-Vaisala frequency, N, for FOAM, left figure, Andrén95, right figure.

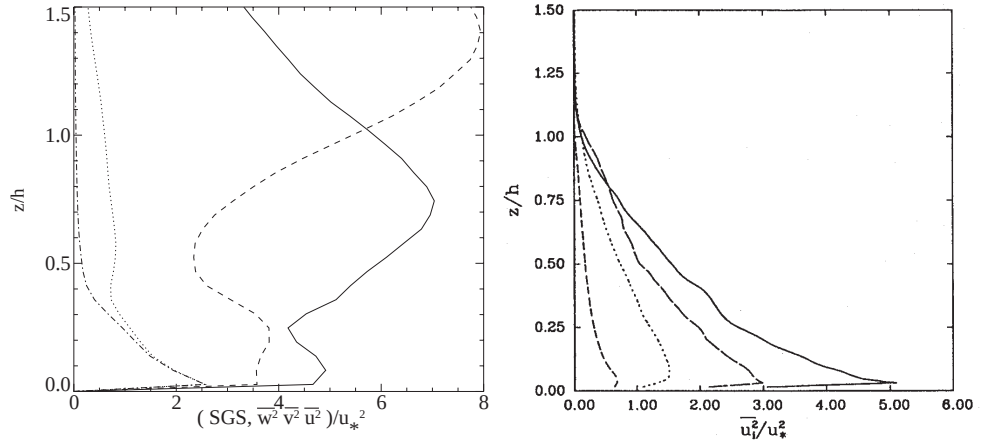

Figure 4.14: The *stable case* (horizontal averages). Wind variances for FOAM (left) and Andrén95 (right). $\overline{u^2}/u_*$ (solid), $\overline{v^2}/u_*$ (long-dashed), $\overline{w^2}/u_*$ (dotted) and SGS part (short-dashed in Andrén95, dash-dotted in FOAM).

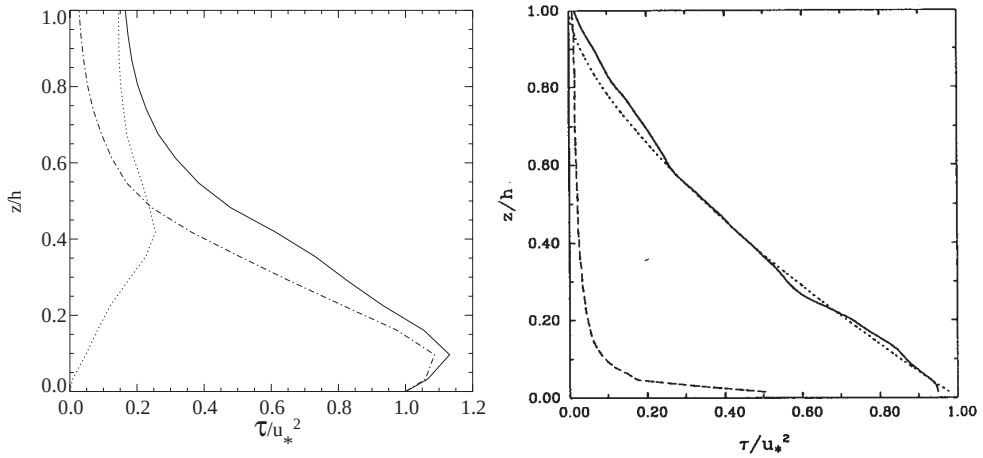

Figure 4.15: The *stable case* (horizontal averages). Flux of Horizontal momentum for FOAM (left figure), total flux (solid), resolved flux (dotted) and SGS flux (dash-dotted). Flux of Horizontal momentum for Andrén95 (right figure), total flux (solid). SGS flux (dashed) and theoretical value (dotted).

probably because of the lack of balance.

For the normalized temperature fluxes in Figure 4.16 can be said that the total flux is similar for FOAM and Andrén95. FOAM has a greater part in the SGS field, again because of the resolution. Here the SGS-model seems to recreate the flux well though.

The conclusion is that it is necessary to perform simulations with much better resolution and for a longer simulation time to verify that FOAM can handle the stable PBL. This is left for the continued evaluation. However, present results indicates that the buoyancy effect included in the code is working in the "right direction".

4.4 The reinfinement of the neutral case.

To annalyse the impact different resolutions makes on the simulation has the neutral case been remade with higher resolution. To compare with the original 40^3 grid was the simulation remade with a 60^3 and a 80^3 grid. The same initial conditions was used and FOAM distributed all initial values from the 40^3 grid to the 60^3 and 80^3 grid with linear interpolation.

These simulations took a great deal longer time to execute because of the substantial increase of gridpoints and therefore increase of calculations. The 60^2 case was simulated for 5 hours with a 3 hour statistic sampling. The 80^2 case was simulated as the 40^2 grid with a 6 hours simulation plus 3 hour sampling of statistics. These differences was made because of the handling of the long and expensive datasimulations but should from a statistic point of wiew be comparable.

Results The overall picture of the differences between the result from different resolutions is that they reproduce the fields very similar. The profile for wind speed and wind direction are very similar (and therefore not included in this report).

The normalized wind variances $\overline{u^2}/u_*$, $\overline{v^2}/u_*$ and $\overline{w^2}/u_*$ for the 60^3 and 80^3 grid can be seen in Figure 4.17 (compare with the 40^3 grid, Figure 4.3). The normalized wind variances for $\overline{v^2}/u_*$ and $\overline{w^2}/u_*$ are similar between the different resolutions. It can be notised that for higher resolution decreases the maxima at the first grid level. With the higher resolution is the maxima for the resolved part larger and situated at lower altitude than for the lower resolution. This follows the basic idea that with

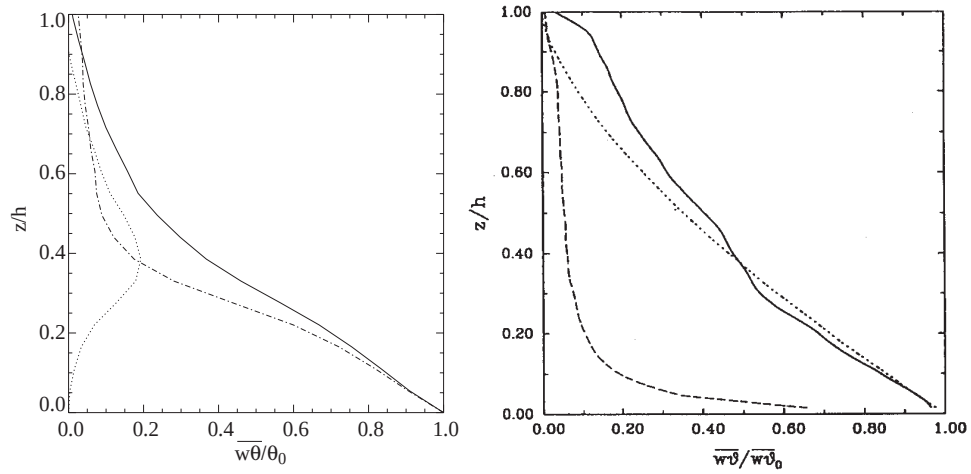

Figure 4.16: The *stable case* (horizontal averages). Temperature flux for FOAM (left figures), total (solid), SGS (dash-dotted) and resolved scale (dotted). Temperature flux for Andrén95, right figures, total (solid) SGS (dashed) and theoretical value (dotted).

finer resolution is more turbulense resolved in the model and less turbulense has to be parameterized. Higher resolution in FOAM works according to theory.

It is important to notise that the subgrid model has used the same constants for all grids, constants that propably need to be adjusted to each specific grid. The wind variances for the $\overline{v^2}/u_*$ and $\overline{w^2}/u_*$ wind shows quite small differences that it's dangerous to draw to big conclusions out of this but it shows that these higher resolution grid does not lead to other problems but includes larger parts of the turbulence in the resolved part of the system. In the 40^3 grid was the maximum value for $\overline{u^2}/u_*$ at the fist gridlevel. This was not the case with the simulations compared by Andrén et al. [1994] where the maximum was at a small altitude above the ground. It was difficult to determine if this was an effect of mistreated boundaryconditions or conditions close to the ground where the eddies are smaller and not all are resolved. In the higher resolution simulations lies the maxima higher which means that this was not the case.

The normalize momentum flux $\overline{uw}$ for the 60^3 and the 80^3 grid is plotted in Figure 4.18. There is espesially one feature that can be notised, the minima just above ground level. This minima is stronger for higher resolution and can not be seen in the 40^3 grid, Figure 4.4. It is difficult to say if this happens because of some misstreatment of the boundarycondition, but when the eddies are small close to the ground the u-momentum flux seem to be to large.

The Monin-Obukhov similarity function is plotted in Figure 4.19 for the three different grids. A higher resolution gives a slightly better Φ which is nice.

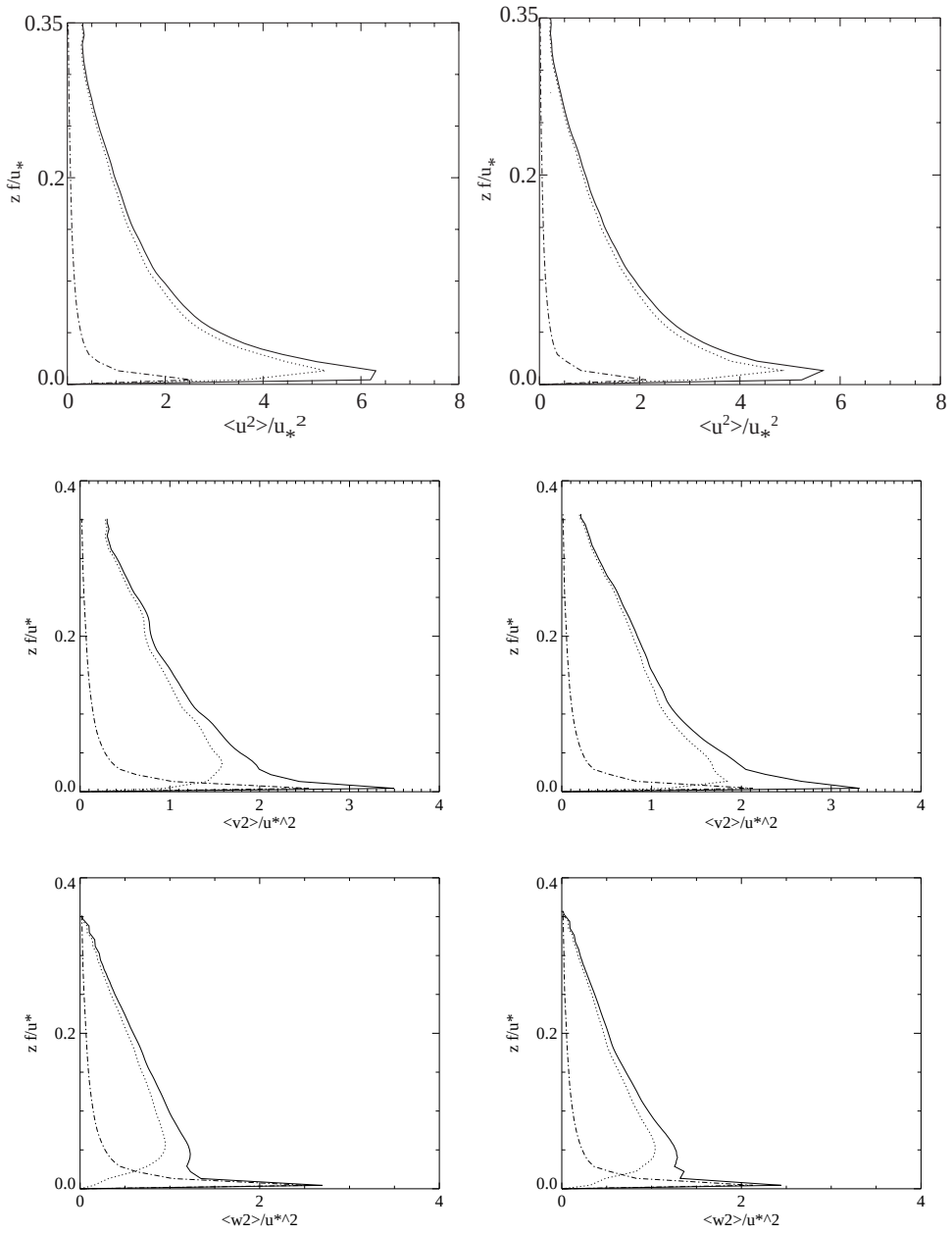

Figure 4.17: The *higher resolution* cases. Normalized wind variances for the u, v and w wind. The 60^3 grid to the left and the 80^3 grid to the right. Total variance (solid), resolved part (dashed) and SGS part (dash-dotted). Compare with the40^3 grid, Figure 4.3.

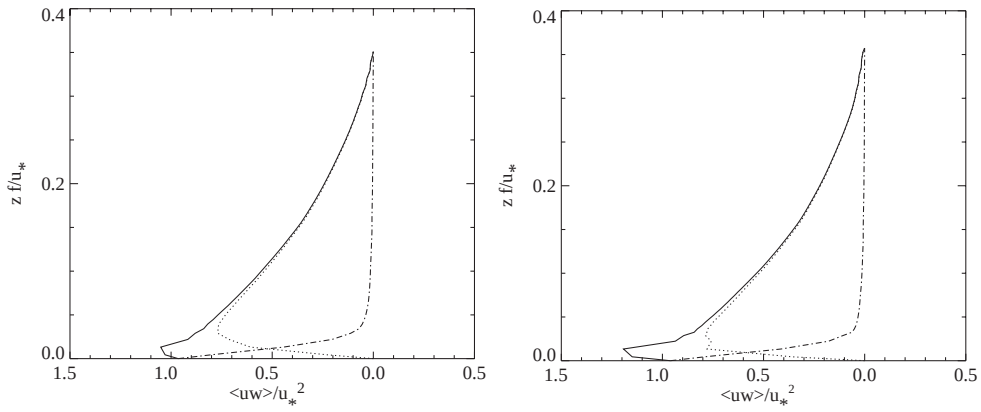

Figure 4.18: The *higher resolution* cases. Normalized momentum flux for the u wind. The 60^3 grid to the left and the 80^3 grid to the right. Total variance (solid), resolved part (dashed) and SGS part (dash-dotted). Compare with the 40^3 grid, Figure 4.4.

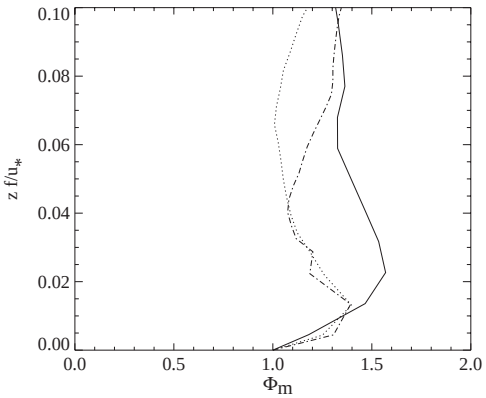

Figure 4.19: Monin-Obukhovs similarity function, Φ_m, for the different grids. 40^3 grid (solid) 60^3 grid (dashed) and 80^3 grid (dash-dotted). Compare with the 40^3 grid, Figure 4.2.

5. Summary

The first steps in validating FOAM for the atmospheric boundary layer have been taken. Many things are indicating that FOAM can be considered a functional LES for PBL simulations if it is set up correctly.

For the neutral boundary layer FOAM creates fields with a large correlation compared to previous neutral PBL simulations. Slightly less wind variances or turbulence can be noticed. Wether this is a consequence of the different numerical scheme in the vertical (FOAM uses non-staggered grid, while all simulations in Andrén et al. [1994] have used staggered grids) or has other causes is not clarified. However, the differences are so small, that it is impossible to judge wether FOAM is better or worse than previous simulations compared to reality. The neutral case was close to a steady state, perhaps with a small reminiscence of an inertial oscillation. This case had in principal been run for 39 hours which should be enough time for a neutral simulation. However, the original field was far from balanced so this long simulation time was necessary.

The convective boundary layer has historically been the most successful boundary layer to simulate. The FOAM simulation demonstrates that the implemented buoyancy forces is clearly working in the "right direction", but also that the set up of the simulations has to be made more carefully. In the further evaluation of FOAM for the convective PBL a capping inversion, that limits the growth of the convective PBL, will be used. Also longer simulations are necessary.

The same is true for the stable boundary layer but in this case better computational resources are necessary since the number of grid points has to be increased substantially. The simulation also has to be much longer so that the flow may reach a steady state. The simulation made for the stable PBL were almost no large eddy simulation, since e.g. major parts of the fluxes of heat and momentum was taken care of in the SGS model. The computer resources needed to make a "real" stable PBL simulation will hopefully be available within the next few months.

The SGS model that is to be used in FOAM in the future is a very important issue for investigation since it is a crucial part of the LES. A SGS model that could handle horizontal inhomogeneities, fields with stable and unstable areas, different grids and that is not too computational expensive is desirable. FOAM is in the future going to simulate the PBL over a city why these features are of greatest importance for the whole LES. The next step here is, after the validation, to insert an object in the flow.

FOAM is at the moment under development for PBL flows and this is a first step in that work. There are things to be done in the future with both validation and development but everything is pointing in the direction that FOAM is behaving well, according to the theory of the planetary boundary layer.

Acknowledgements Many thanks to my supervisors Michael Tjernström and Lennart Thaning for all support and encouragement even at irregular hours. Many thanks to Leif Persson who helped me with C++, LaTeXand all my other questions. Thanks to Rezwan Mohammad, for all the help with LaTeX.

Bibliography

A Andrén. The structure of stably stratified atmospheric boundary layers: A large-eddy simulation study. *Q.J.R. Meteorological Society*, 121:961–985, 1995.

A Andrén, A.R. Brown, J. Graf, Mason P.J., C.-H. Moeng, F.T.M. Nieuwstadt, and U. Schuman. Large-eddy simulation of a neutrally stratified boundary layer: A comparison of four computer codes. *Q.J.R Meteorological Society*, 120:1457–1484, March 1994.

S. Paul Arya. *Introduction to Micrometeorology*, volume 42 of *International geophysics series*. Academic Press, Inc., 1988. ISBN 2-12-064490-8.

J.W. Deardorff. The use of subgrid transport equations in a three-simentional model of atmospheric turbulence. *J.Fluids Eng.*, 95:429–438, September 1973.

J.W. Deardorff. Three-dimensional numerical study of the height and mean structure of a heated planetary boundary layer. *Boundary - Layer Meteorology*, 7:81–106, 1974.

J.W. Deardorff. Stratocumulus-capped mixed layers derived from a three-dimensional model. *Boundary - Layer Meteorology*, 18:405–527, 1980.

James R. Holton. *An introduction to dynamic meteorology*, volume 48 of *International geophysics series*. Academic Press, Inc., third edition, 1992. ISBN 0-12-354355-X.

Hjvoje Jasak. Improving the accuracy of numerical solution procedures in computational fluid dynamics. Technical report, Dept. of Mechanical Engineering, Imperial College of Science, Thecnology and Medicine, August 1995.

Chin-Hoh Moeng. A large-eddy-simulation model for the study of planetary boundary-layer turbulence. *Journal of the Atmospheric Sciences*, 41(13):2052–2062, may 1984.

Roland B. Stull. *An Introduction to Boundary Layer Meteorology* Kluwer Academic Publishers, 1988. ISBN 90-277-2769-4.

Peter P. Sullivan, James C. Mc Williams, and Chin-Hoh Moeng. A subgrid-scale model for large-eddy simulation of planetary boundary-layer flows. *Boundary-Layer Meteorology*, 71:2052–2062, April 1994.

H.G. Weller, G. Tabor, H. Jasak, and C. Fureby. A tensorial approach to computational continuum mechanics using object orientated techniques. *Computers in Physics*, 12(6):620–631, November/December 1998.

H.G. Weller et al. FOAM a C++ class library for continuum mechanics. FOAM paper, Version 1.7 β, July 1998.

6. Appendix

6.1 Tensor Notation

In the paper the Einstein's summation notation is used [Stull, 1988, section 2.8]. Conventions for this tensor notation are as.

- A variable with *no* free indices is a *scalar*.
- A variable with *one* free indices is a *vector*.
- A variable with *two* free indices is a *tensor*.

Prescribed tensors:

- The Kronecker Delta, δ_{ij}, (a scalar quantity even if it has two indices)

$$\delta_{ij} = \begin{pmatrix} 1 & 0 & 0 \\ 0 & 1 & 0 \\ 0 & 0 & 1 \end{pmatrix}$$

- The Alternating Unit Tensor, ε_{ijk}, (a scalar quantity even if it has three indices)

$$\varepsilon_{ijk} = \begin{cases} +1 & i,j,k = (1,2,3);(2,3,1);(3,1,2) \\ -1 & i,j,k = (3,2,1);(2,1,3);(1,3,2) \\ 0 & \text{otherwise} \end{cases}$$

- The Coordinate vector $x_i = (x, y, z)$
- The Velocity vector $u_i = (u, v, w)$

There are three fundamental rules in summation notation:

1. When two identical indices appear in the same term. Summation is made over that term for each value (1,2,3) of the repeated index.
2. When one index appears not summed (free) in one term that same index must appear not summed in all terms of that equation. The equation then represents three equations for each value of the not summed index.
3. The same index cannot appear more than twice in the same term.

6.2 Stress Tensors

The viscous stress tensor may be written as: [Stull, 1988, section 2.9].

$$\tau_{ij_{visc}} = -\nu \left(\frac{\partial u_i}{\partial x_j} + \frac{\partial u_j}{\partial x_i} \right) + \left(\mu_B - \frac{2}{3}\mu \right) \frac{\partial u_k}{\partial x_k} \delta_{ij} \tag{6.1}$$

where μ_B is the bulk eddy viscosity coefficient and μ is the dynamic viscosity coefficient. It is assumed that the turbulent viscosity can be parameterized in a similar way.

$$\overline{u_i' u_j'} = \begin{pmatrix} \overline{u'^2} & \overline{u'v'} & \overline{u'w'} \\ \overline{v'u'} & \overline{v'^2} & \overline{v'w'} \\ \overline{w'u'} & \overline{w'v'} & \overline{w'^2} \end{pmatrix} = -K_m \left(\frac{\partial \bar{u}_i}{\partial x_j} + \frac{\partial \bar{u}_j}{\partial x_i} \right) + \frac{2}{3}\bar{e}\delta_{ij} \tag{6.2}$$

where K_m is the turbulent viscosity coefficient and $\bar{e}$ is the sub grid scale turbulent kinetic energy.